ACADEMIA ROMÂNĂ
Revue Roumaine de Chimie
http://web.icf.ro/rrch/

Rev. Roum. Chim.,
2018, *63*(5-6), 393-400

Dedicated to Dr. Maria Zaharescu
on the occasion of her 80th anniversary

INFLUENCES OF Ba/Sr RATIO AND Mn DOPING ON MICROWAVE DIELECTRIC PROPERTIES OF $Ba_xSr_{1-x}TiO_3$ THIN FILMS

Tanja PEČNIK,[a] Sebastjan GLINŠEK,[b] Brigita KMET[a] and Barbara MALIČ[a]

[a] Electronic Ceramics Department, Jožef Stefan Institute, Jamova cesta 39, 1000 Ljubljana, Slovenia
[b] Materials and Research Technology Department, Luxembourg Institute of Science and Technology, 41 Rue du Brill, L-4422 Belvaux, Luxembourg

Received September 14, 2017

The Ba/Sr ratio and manganese doping influence dielectric permittivity and losses of $Ba_xSr_{1-x}TiO_3$ films in GHz range and are thus important when designing materials for tunable microwave-range applications. The $Ba_xSr_{1-x}TiO_3$ films, with x=0.5 (BST 50/50), 0.4 (BST 40/60) and 0.3 (BST 30/70) were prepared from acetate-alkoxide based precursor solutions. The films crystallize in perovskite phase with columnar microstructures after annealing at 900 °C. The room-temperature 10 GHz dielectric permittivity of the BST 50/50 film is 1310 and it drops to 680 for the BST 30/70 film, in line with the drop of voltage tunability (at 40 V) from 3.3 to 1.5. In parallel, dielectric losses decrease from 0.14 to 0.03. Very similar characteristics are observed for manganese doping of Ba-rich BST films. Combination of both approaches is efficient strategy to tune dielectric response of BST films for applications in microwave circuits.

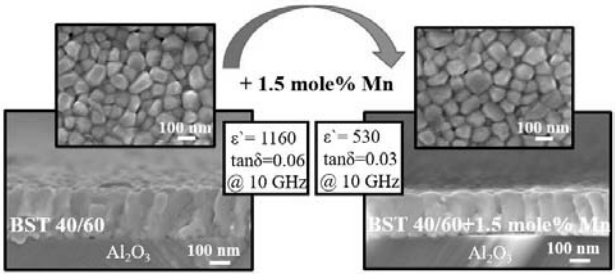

INTRODUCTION

Ferroelectric materials are attractive for microwave devices, such as antennas, tunable phase shifters or filters, due to the ability to change their dielectric permittivity by an external electric field and because of relatively low dielectric losses at microwave frequencies. The electric-field-dependent dielectric permittivity is commonly described by the tunability (n), defined as the ratio of the dielectric permittivity at zero electric field bias to the permittivity at a selected electric field bias.[1,2]

Barium strontium titanate $Ba_xSr_{1-x}TiO_3$, x=0-1 (BST or BST 100x/100(1-x)) is by far the most studied material for these applications. The ferroelectric to paraelectric transition temperature, marked by the peak in dielectric permittivity, varies by changing the Ba/Sr ratio from 0 to 1 in temperature interval from 0 to 390 K. Compositions in the paraelectric phase at the operating temperatures, but nevertheless close to the permittivity maximum, exhibit high tunability and low dielectric losses at microwave frequencies.[1–4]

Ferroelectric materials are used as bulk materials, thick or thin films. The application of bulk materials requires tuning voltages in the order of kVs. It can be strongly reduced by using thin films, which also enables easier integration and

* Corresponding author: tanja.pecnik@ijs.si

substantial miniaturization of the devices. The BST thin films with thicknesses of several hundred nanometers have been prepared by various deposition techniques, such as pulsed laser deposition, magnetron sputtering, metal organic chemical vapor deposition and chemical solution deposition (CSD) (see Ref.[3] and references therein, [5–11]). Properties of the films usually deviate from the ones reported for bulk materials. Several, usually simultaneous effects, are responsible, such as different stoichiometry and levels of homogeneity, increased concentration of defects within the crystal structure, presence of layers with different dielectric properties on both surfaces of the film, electrode-film interaction and non-zero strain of the films clamped to the substrate.[2,3]

In our previous work, we studied dielectric properties of the solution-derived BST 50/50 films in the thickness range from 90 nm to 400 nm[12]. The films on polycrystalline alumina substrates were prepared by repeated spin coating and rapid-thermal-annealing steps of a few 10 nm-thick deposited layers at 900 °C, until the required thickness was reached. The 240 nm-thick film had a dense, uniform columnar microstructure and exhibited the highest dielectric permittivity of 1350, losses of 0.02 and voltage tunability of 3.3, all at 100 kHz. At 15 GHz the permittivity was only slightly lower, 1300. The radiation hardness studies revealed that such films survive both neutron and gamma-ray irradiation levels exceeding the largest expected levels of ionizing and non-ionizing exposure during satellite missions without noticeable change in their microwave response.[13] As such they are compatible with applications in frequency-agile antennas for satellite missions.[14] However, the problem of relatively high losses (0.16 at 15 GHz) remained to be solved.[12]

The aim of this work was to investigate two approaches to reduce dielectric losses of the BST films, namely by increasing the fraction of strontium in the solid solution, *i.e.*, decreasing the Ba/Sr molar ratio; and secondly, by doping selected solid solutions with manganese. Manganese has been previously reported to efficiently reduce the dielectric losses and leakage current density of different ferroelectric perovskite thin films such as BST[15,16], $(K_{0.5}Na_{0.5})(Nb_{0.8}Ta_{0.2})O_3$[17], $((Na_{0.85}K_{0.15})_{0.5}Bi_{0.5})TiO_3$[18], $(K_{0.5}Na_{0.5})NbO_3$-$CaZrO_3$[19], and $Pb(Zr_{0.52}Ti_{0.48})O_3$[20]. In this work the phase composition, microstructure, kHz- and GHz-range dielectric properties of BST films with Ba/Sr ratios 50/50 (used as reference, see[12]), 40/60, 30/70, and manganese-doped BST 50/50 and 40/60 films are reported.

EXPERIMENTAL

The solutions for BST thin films with different compositions, *i.e.*, BST 50/50, 40/60, and 30/70 were prepared from the alkaline earth acetates ($Ba(CH_3COO)_2$, 99.999%, Alfa Aesar; $Sr(CH_3COO)_2$, 99.81%, Alfa Aesar) and Ti-butoxide ($Ti(OC_4H_8)_4$, 99.61%, Fluka). In selected cases manganese acetate ($Mn(CH_3COO)_2$, 98+ %, Alfa Aesar) was added in order to obtain 0.5, 1.0 and 1.5 mole% doping (calculated as B-site substitution) of BST solutions. All acetates were dried before use and then dissolved in acetic acid (100%, Merck). Ti-butoxide was diluted by the 2-methoxyethanol ($CH_3OCH_2CH_2OH$, 99.3+ %, Sigma Aldrich). The two solutions were mixed for 2 hours at room temperature and the concentration of the solutions was adjusted to 0.25 M. The details are described in our previous work.[12]

The films of approximately the same thicknesses were prepared on polished alumina substrates (99.6 %, 3.95 g/cm^3, 25.4 mm x 25.4 mm x 0.26 mm, Coorstek) by a multi-step annealing process at 900 °C as schematically presented in Fig. 1. The first step was deposition of the solutions on the substrate, drying at 200 °C for 2 min, pyrolysis at 350 °C for 2 min and annealing at 900 °C for 15 min in a rapid thermal annealing furnace (TM100-BT, LPT, Germany), with the heating rate of 15 K/s. For intermediate layers, the time of annealing after drying and pyrolysis was 5 min and for the final step 60 min. After repeating seven deposition-drying-pyrolysis-annealing steps achieved film thicknesses, as determined from cross-section micrographs of Field Emission Scanning Electron Microscope (FE-SEM, JSM-7600F, Jeol), were around 240 nm for all the films.

The phase composition of all films was determined by PANalytical X'Pert PRO MPD X-ray diffractometer (XRD, PANalytical, Netherlands) with $CuK_{\alpha 1}$ radiation. The XRD patterns were recorded in a 2θ region from 20 ° to 50 ° with the step of 0.017 °, the exposure time of 100 s and with a capture angle of 2.122 °. The microstructure of thin films was analyzed by FE-SEM. The average grain sizes of the films were determined by stereological analysis of FE-SEM surface micrographs on approximately 380 grains (Image Tool 3.0, University of Texas Health Science Center at San Antonio).

For the kHz-range dielectric characterization the planar capacitor structures with 3 μm-sized gaps were patterned using the lift-off photolithography and Cr/Au electrodes were deposited by magnetron sputtering (5Pascal, Italy). The capacitance and dielectric losses of BST thin films were measured by Impedance Analyzer (HP 4284 A, Keysight, USA) at 100 kHz and at room temperature. Capacitance-voltage characteristics, measured at 100 kHz, were recorded with the following DC biasing scheme: 0V → + 40 V → 0 V → - 40 V → 0 V. The dielectric permittivity of the BST films was calculated by applying the partial capacitance method (PCM).[21,22] The dielectric permittivity of the film ε_f is expressed as:

$$\varepsilon_f = \varepsilon_s + \left(\frac{s}{h_f} + \frac{4}{\pi} \ln 2 \right) \left[\frac{C_m}{\varepsilon_0 w} - \frac{2}{\pi} \ln\left(\frac{4l}{s} \right) - \frac{\varepsilon_s - 1}{\pi} \ln\left(16 \frac{h_s}{\pi s} \right) \right],$$

where C_m is measured capacitance, ε_s is permittivity of the alumina substrate, s is gap between the electrodes, h_f is thickness of the film, ε_0 is permittivity of the vacuum, w is length of the electrodes, l is width of two electrodes and h_s is thickness of the substrate.

Split-post dielectric resonators (QWED, Poland) connected to a Network Analyzer (HP 8720 ES, Keysight, USA) were used to analyze the dielectric properties of the BST films at 10 and 15 GHz.

RESULTS AND DISCUSSION

1. BST films with different Ba/Sr ratios

The BST films 50/50, 40/60 and 30/70 crystallize in perovskite phase upon annealing at 900 °C, see Fig. 2. As the Ba/Sr molar ratio decreases the perovskite peaks shift towards higher 2θ angles which indicates decreasing of the lattice parameters with increasing amount of strontium.[10,23] The shifting of the (110) perovskite peaks is shown in detail in Fig. 3.

The cross-section and surface microstructures of BST films and the average lateral grain sizes (GS) obtained from the FE-SEM analysis are presented in Fig. 4. All investigated films consist mainly of columnar grains. The dense in-plane microstructures of the BST films are related to the multi-step heat treatment where each individual deposit is annealed after drying and pyrolysis[12], which is in agreement with earlier studies, cf [5,24]. Stereological analysis showed that the addition of Sr resulted in a gradual decrease of the grain size (Fig. 4). The average grain sizes of BST 50/50, BST 40/60 and BST 30/70 are 87, 83 and 81 nm with standard deviations of 22, 21 and 29 nm, respectively. The change in the average grain size of different compositions might be related to the fact that the melting temperature of strontium titanate (T_{melt} = 2080 °C) is higher than the melting temperature of barium titanate (T_{melt} = 1618 °C). Consequently, nucleation and grain growth processes of the perovskite occur at higher temperatures for strontium-rich compositions, resulting in microstructures with smaller grains.

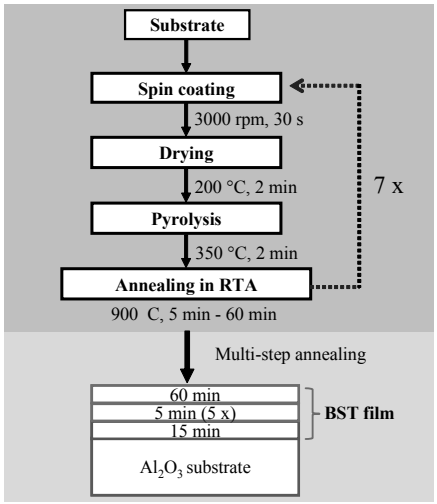

Fig. 1 – Schematic presentation of the thin-film deposition by multi-step annealing.

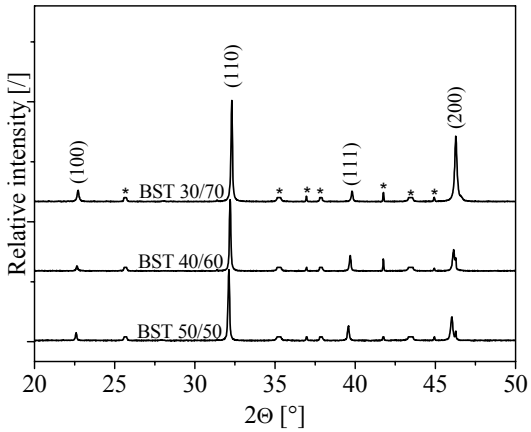

Fig. 2 – XRD patterns of BST 50/50, BST 40/60 and BST 30/70 thin films on alumina substrates. The peaks of alumina (JCPDS 01-081-226) were subtracted and are denoted by *. The main reflections of the perovskite structure are indexed according to the reference for BST 50/50 (JCPDS 00-039-1395).

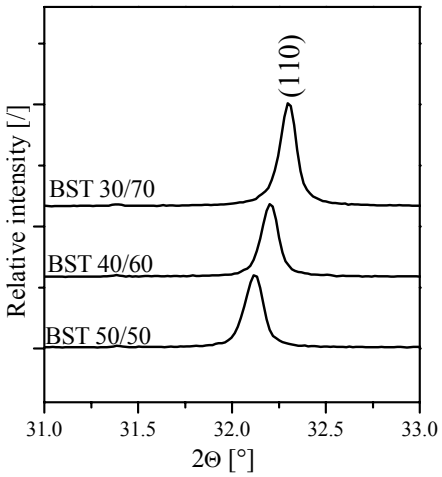

Fig. 3 – XRD patterns of BST films with different Ba/Sr molar ratios in a narrow 2θ range showing (110) peaks of the perovskite phase.

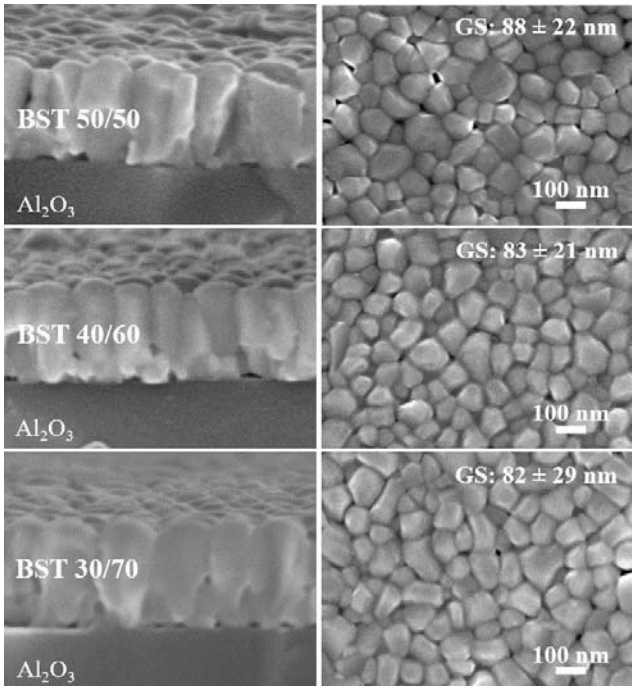

Fig. 4 – FE-SEM micrographs of the cross-section and plane-view microstructures with average grain sizes (GS) of approximately 240 nm-thick BST 50/50, 40/60 and 30/70 thin films on alumina substrates.

The dielectric permittivity and losses of all thin films measured at 100 kHz, 10 GHz and 15 GHz and at room temperature (RT) are presented in Fig. 5. The 100 kHz-dielectric permittivity decreases with decreasing Ba content from 1350 for BST 50/50 to 680 for BST 30/70. The same trend, with slightly lower values, is observed also in the GHz range, namely, the 10 GHz values of permittivity for BST 50/50 and 30/70 films are 1310 and 680. The decrease of the permittivity with decreasing Ba/Sr molar ratio is explained with the composition-dependent Curie temperature, with respective values for BST 50/50, 40/60 and 30/70 bulk ceramics -30 °C, -60 °C, and -100 °C[2]. Generally high permittivity values of the films are due to dense and uniform columnar microstructure of the films.[12] Hoffmann *et al.*[5] observed that $BaTiO_3$ films with the columnar microstructure had higher dielectric permittivity compared to grainy and porous ones. The observation was confirmed by Aygün *et al.* for $BaTiO_3$ films[8] and Kageyama *et al.* for BST 70/30 films[7]. In a study of BST 70/30, 50/50 and 30/70 films on Pt/Si substrates Levasseur *et al.* showed that annealing at 800 °C resulted in larger grains, reduced porosity and in enhanced dielectric properties as compared to annealing at 600 °C; in BST 50/50 films the 10 kHz-permittivity increased from 150 to 260.[25]

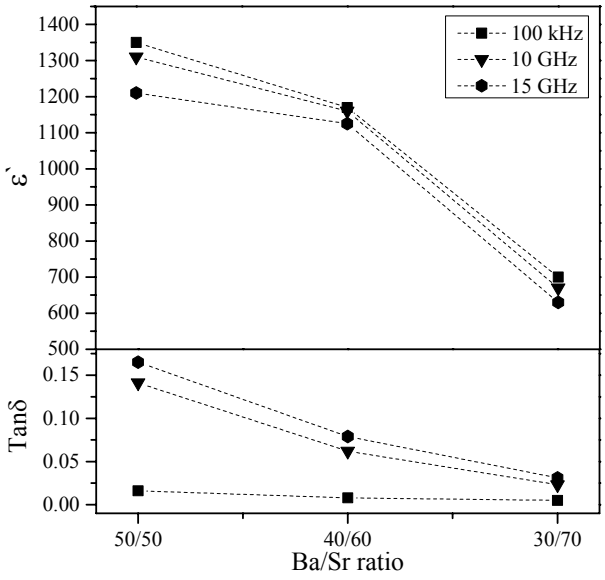

Fig. 5 – Room-temperature dielectric permittivity and losses of approximately 240 nm-thick BST 50/50, 40/60 and 30/70 thin films measured at 100 kHz, 10 GHz and 15 GHz. Lines are guides to the eye.

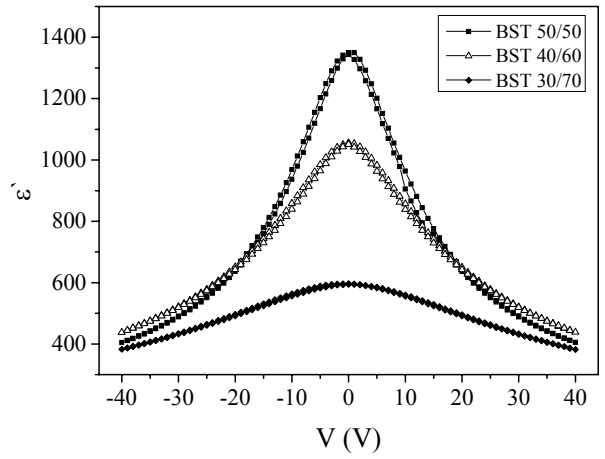

Fig. 6 – Voltage dependence of the dielectric permittivity measured at 100 kHz for BST 50/50, 40/60 and 30/70 thin films.

As also shown in Figure 5 is the change of composition from BST 50/50 to BST 30/70, which resulted in significantly lower dielectric losses measured at microwave frequencies. The 10 GHz-losses of BST 50/50 thin films are 0.14 and they decrease to 0.03 in BST 30/70. Strong dispersion of the losses observed in BST 50/50, which gradually decrease with increasing concentration of strontium, is probably related to polar regions, whose relaxation is expected to appear in the GHz region.[26]

Voltage dependence of the permittivity of BST films measured at 100 kHz and room temperature is presented in Fig. 6. Tunability, *n*, is expressed as the ratio of permittivities at 0 V and 40 V. The highest value of 3.3 is obtained for the BST 50/50 film and is related to its highest zero-field permittivity. With decreasing Ba/Sr ratio the tunability gradually decreases to 2.4 and 1.6 for BST 40/60 and 30/70, respectively.

2. Manganese doped BST films

We further investigated the influence of manganese doping on microstructure and dielectric properties of BST 50/50 and 40/60 films, which exhibited high values of dielectric permittivity and tunability but also high dielectric losses in the GHz range. The mole fractions of manganese were 0.5, 1 and 1.5 mole %, similar range as was found to be effective in studies of different complex perovskites.[16,17,19,20,27]

We found that the addition of up to 1.5 mole % Mn had a similar effect on phase composition and microstructure of both BST films upon annealing at 900 °C, therefore we only show the results for BST 40/60. All manganese-modified films crystallize in pure perovskite phase as shown in Fig. 7. A slight change in the degree of preferred crystallographic orientation is observed; the unmodified BST 40/60 films are randomly oriented and they become slightly (200)-oriented with increasing Mn content, as observed from the increased ratio of relative intensities of the (200) and (110) perovskite diffraction peaks.

The FE-SEM cross-section and surface microstructures of the films are collected in Fig. 8. All films have dense cross-sectional microstructures with predominantly columnar grains. Average lateral grain size is about 80 nm and no clear trend with increasing manganese addition can be deduced from the plane-view micrographs. The observation is consistent with the literature, in which no changes in the density, shape or size of the grains were reported for manganese-doped BST thin films.[15,16,27]

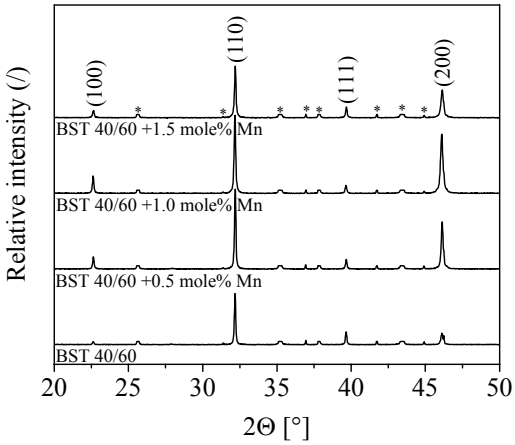

Fig. 7 – XRD patterns of BST 40/60 thin films with 0, 0.5, 1.0 and 1.5 mole % of Mn prepared on alumina substrates. * - diffraction peaks of alumina substrate.

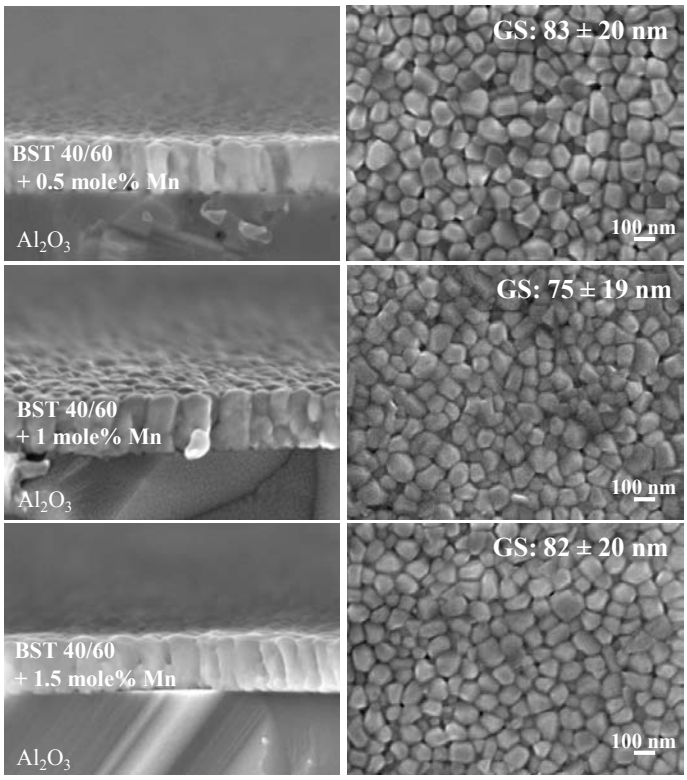

Fig. 8 – FE-SEM micrographs of the cross-section and plane-view microstructures of BST 40/60 thin films with 0 (already shown in Fig. 4), 0.5, 1.0 and 1.5 mole % Mn prepared on alumina substrates.

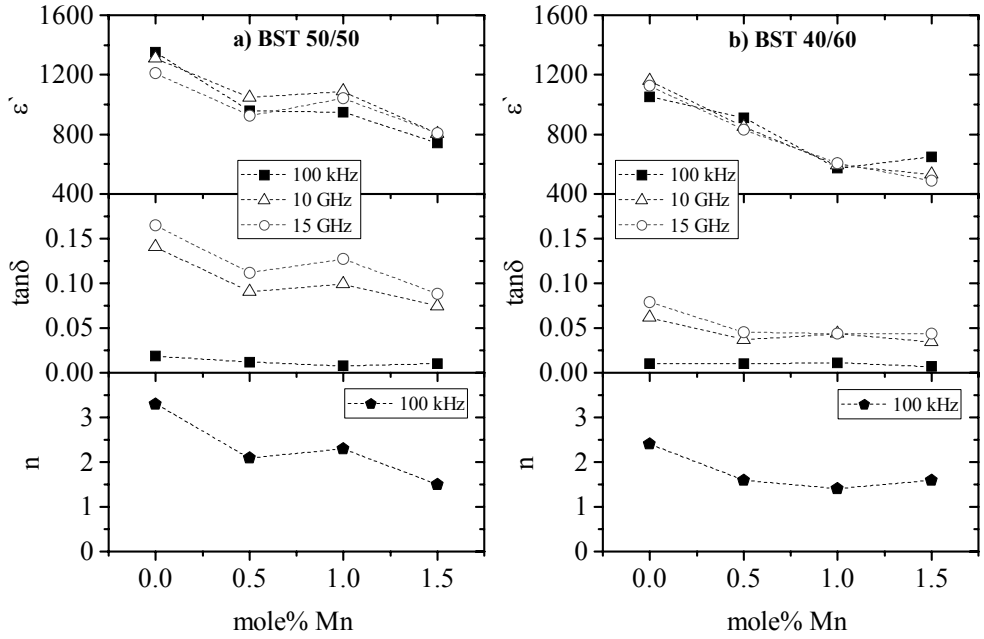

Fig. 9 – Dielectric permittivity (*ε`*), dielectric losses (tan*δ*) and tunability (*n*) of undoped and doped a) BST 50/50 and b) BST 40/60 films, measured at 100 kHz, 10 GHz and 15 GHz. Tunability is expressed as the ratio of permittivities at 0 and 40 V.

The dielectric permittivity and losses of Mn-modified BST 50/50 and 40/60 films measured at 100 kHz, 10 and 15 GHz together with tunability values at 100 kHz are collected in Fig. 9. The 100 kHz permittivity of the BST 50/50 film is 1350 and it decreases to around 950 for the films doped with 0.5 and 1 mole% Mn. With increasing amount of dopant to 1.5 mole% the permittivity further decreases to 740. Its 15 GHz value for the undoped films is 1210 and it decreases to 810 for the 1.5 mole% Mn. The kHz-range dielectric losses of undoped BST 50/50 film are 0.02 and they remain below 0.01 with manganese doping. A strong increase of the absolute value is observed at higher frequency, i.e., 0.17 and 0.09 for the undoped and 1.5 mole% doped films at 15 GHz, respectively. Voltage tunability decreases also from 3.3 for undoped BST 50/50 films to 1.5 for the film with 1.5 mole% of Mn.

The same trend with decreasing dielectric permittivity, losses and tunability with increasing amount of manganese dopant is observed also for the BST 40/60 films, however, the absolute values of the permittivity and losses are lower as compared to the BST 50/50 films. The disparity is explained by the difference in Curie temperature, as discussed in previous section. The BST 40/60 films doped with 1.5 mol% of manganese have the 15 GHz values of permittivity and losses 490 and 0.04, respectively, but the tunability of 1.4 is comparable to BST 50/50 with the same amount of manganese.

Nadaud *et al.*[27] investigated the effect of manganese doping in the case of solution-derived BST 80/20 thin films and found decreased kHz-range dielectric permittivity and losses from 410 and 0.03 for undoped film to 380 and 0.016 for the films doped with 1 mol% Mn. Such behavior is ascribed to the acceptor doping at B-site, which partially substitutes the titanium ions and compensates the electrons released by the oxygen vacancies. As a consequence extrinsic dielectric losses strongly decrease.[27]

CONCLUSIONS

In this contribution the effect of composition and manganese doping on phase composition, microstructure and dielectric properties of the solution-derived $Ba_xSr_{1-x}TiO_3$ thin films, with x = 0.5 (BST 50/50), 0.4 (BST 40/60) and 0.3 (BST 30/70) has been studied.

According to the XRD analysis, all undoped BST films crystallize in perovskite phase after annealing at 900 °C and have dense and uniform in-plane microstructures with mostly columnar grains. The films are characterized with high dielectric permittivity values, *e.g.*, 1310 for BST 50/50 measured at 10 GHz and room temperature. As the Ba/Sr ratio decreases to 30/70 the dielectric permittivity decreases to 680, which is in agreement with the composition-dependent Curie temperature of the films. Tunability, expressed as

the ratio of 100 kHz permittivities at 0 and 40 V, and dielectric losses decrease from 3.3 to 1.5 and from 0.14 to 0.03, respectively.

Doping with up to 1.5 mole% of Mn does not significantly affect the phase composition or microstructure of BST 50/50 and 40/60 films. However, in BST 40/60 a drop of the 15 GHz-range dielectric permittivity from 1125 to 490 as the films were doped with 1.5 mole% of Mn, is observed, with dielectric losses 0.04 and moderately high 100 kHz tunability (1.4). Similar trend was also observed in BST 50/50 films.

The results demonstrate that tuning via Ba/Sr ratio and manganese doping are efficient strategies to obtain high tunability and simultaneously low dielectric losses in GHz frequency range, which is essential for their implementation into tunable microwave devices.

Acknowledgments: This work was supported by the Slovenian Research Agency (P2-0105, PR-05026 and J2-5482) and European Space Agency in the frame of the ESA-PECS project FERROPATCH. SG would like to thank to the Luxembourg National Research Fund for financial support (grant number: FNR/P12/4853155/Kreisel).

REFERENCES

1. M. J. Lancaster, J. Powell and A. Porch, *Supercond. Sci. Technol*., **1999**, *11*, 1323-1334.
2. A. K. Tagantsev, V. O. Sherman, K. F. Astafiev, J. Venkatesh and N. Setter, *J. Electroceramics*. **2004**, *11*, 5-66.
3. P. Bao, T. J. Jackson, X. Wang and M. J. Lancaster, *J. Phys. D Appl. Phys*. **2008**, *41*, 63001-1-21.
4. X. Zhu, J. Zhu, S. Zhou, Z. Liu, N. Ming, S. Lu, H. Lai-Wah Chan and C. L. Choy, *J. Electron. Mater*. **2003**, *32*, 1125-1134.
5. S. Hoffmann and R. Waser. *J. Eur. Ceram. Soc*. **1999**, *19*, 1339-1343.
6. S. M. Aygün, P. Daniels, W. Borland and J. P. Maria, *J. Mater. Res*. **2009**, *25*, 427-436.
7. K. Kageyama, A. Sakurai, A. Ando and Y. Sakabe, *J. Eur. Ceram. Soc*. **2006**, *26*, 1873-1877.
8. S. M. Aygün, J. F. Ihlefeld, W. J. Borland and J. P. Maria, *J. Appl. Phys*. **2011**, *109*, 34108-1-5.
9. B. Malič, I. Boerasu, M. Mandeljc, M. Kosec, V. Sherman, T. Yamada, N. Setter and M. Vukadinovic, *J. Eur. Ceram. Soc*. **2007**, *27*, 2945-2948.
10. M. C. Gust, L. A. Momoda, N. D. Evans, M. L. Mecartney, *J. Am. Ceram. Soc*. **2001**, *84*, 1087-1092.
11. A. R. Damodaran, S. Pandya, Y. Qi, S. L. Hsu, S. Liu, C. Nelson, A. Dasqupta, P. Ercius, C. Ophus, L. R. Dedon, J. C. Agar, H. Lu, J. Zhang, A. M. Minor, A. M. Rappe and L. W. Marin, *Nat. Commun*. **2017**, *8*, 1-8.
12. T. Pečnik, S. Glinšek, B. Kmet and B. Malič, *J. Alloys. Compd*. **2015**, *646*, 766-772.
13. S. Glinšek, T. Pečnik, V. Cindro, B. Kmet, B. Rožič and B. Malič, *Acta Mater*. **2015**, *88*, 34-40.
14. V. Furlan, S. Glinšek, B. Kmet, T. Pečnik, B. Malič and M. Vidmar, *IEEE Trans. Microw. Theory. Tech*. **2015**, *63*, 1-6.
15. M. Jain, S. B. Majumder, R. S. Katiyar, F. A. Miranda and F. W. Van Keuls, *Appl. Phys. Lett*. **2003**, *82*, 1911-1913.
16. Z. Yuan, Y. Lin, J. Weaver, X. Chen, C. L. Chen, G. Subramanyam, J. C. Jiang and E. I. Meletis, *Appl. Phys. Lett*. **2005**, *87*, 152901-1-152901-152901-3.
17. N. Kondo, W. Sakamoto, B-Y. Lee, T. Iijima, J. Kumagai, M. Moriya and T. Yogo, *Jpn. J. Appl. Phys*. **2010**, *49*, 09MA04-1-09MA04-6.
18. Y. Wu, X. Wang, C. Zhong and L. Li, *J. Am. Ceram. Soc*. **2011**, *94*, 3877-3882.
19. T. Matsuda, A. W. Sakamoto, B. Lee, T. Iijima and J. Kumagai, *Jpn. J. App.l Phys*. **2012**, *51*, 09LA03-1-09LA03-6.
20. W. Zhu, I. Fujii, W. Ren and S. Trolier-McKinstry, *J. Appl. Phys*. **2011**, *109*, 64105.
21. O. G. Vendik, S. P. Zubko and M. A. Nikol'skii, *Tech. Phys*. **1999**, *44*, 349-355.
22. M. Vukadinovič, B. Malič, M. Kosec and D. Križaj, *Meas. Sci. Technol*. **2009**, *20*, 115106-1-11.
23. "PDF 01-071-1241", JCPDS-International Center for Diffraction Data, 2002.
24. B. Malic, M. Vukadinovic, I. Boerasu, M. Mandeljc, E. Ion, M. Kosec, V. Sherman, T. Yamada and N. Setter, *Integr. Ferroelectr*. **2007**, *93*, 119-125.
25. D. Levasseur, H. B. El-Shaarawi, S. Pacchini, A. Rousseau, S. Payan, G. Guegan and M. Maglione, *J. Eur. Ceram. Soc*. **2013**, *33*, 139-146.
26. T. Ostapchuk, J. Petzelt, J. Hlinka, V. Bovtun, P. Kužel, I. Ponomareva, S. Lisenkov, L. Bellaiche, A. Tkach and P. Vilarinho, *J. Phys.: Condens. Matter*. **2009**, *21*, 1-6.
27. K. Nadaud, C. Borderon, R. Renoud and H. W. Gundel, *J. Appl. Phys*. **2015**, *117*, 084104-1-084104-7.